

Time-resolved photoelectron imaging of the iodide–thymine and iodide–uracil binary cluster systems

Sarah B. King,^a Margaret A. Yandell^a and Daniel M. Neumark^{*ab}

Received 22nd December 2012, Accepted 15th February 2013

DOI: 10.1039/c3fd20158a

The energetics and dynamics of thymine and uracil transient negative ions were examined using femtosecond time-resolved photoelectron imaging. The vertical detachment energies (VDEs) of these systems were found to be 4.05 eV and 4.11 eV for iodide–thymine ($I^- \cdot T$) and iodide–uracil ($I^- \cdot U$) clusters, respectively. An ultraviolet pump pulse was used to promote intracluster charge transfer from iodide to the nucleobase. Subsequent electron detachment using an infrared probe pulse monitored the dynamics of the resulting transient negative ion. Photoelectron spectra reveal two primary features: a near-zero electron kinetic energy signal attributed to autodetachment and a transient feature representing photodetachment from the excited anion state. The transient state exhibits biexponential decay in both thymine and uracil complexes with short and long decay time constants ranging from 150–600 fs and 1–50 ps, respectively, depending on the excitation energy. However, both time constants are systematically shorter for $I^- \cdot T$. Vibrational autodetachment and iodine loss are identified as the primary decay mechanisms of the transient negative ions of thymine and uracil.

1 Introduction

Ionizing radiation is a major cause of damage to DNA.^{1,2} Though experiments and theory estimate the lowest ionization potentials for DNA components to be between 8–11 eV,^{3–7} electrons with less than 3 eV of kinetic energy have been demonstrated to induce both single and double strand breaks in DNA.⁸ The mechanism of strand cleavage by ionizing radiation below the relevant ionization potentials has been the subject of much recent study. Theoretical work by Simons⁹ and Schaefer¹⁰ posits that these strand breaks result from electron attachment to the empty π^* orbital of the nucleobase followed by energy transfer and cleavage of the C–O σ bonds in the sugar phosphate backbone of the DNA strand. Cleavage of the N–C bond linking the sugar to the nucleobase at the N1 position (Fig. 1) and N–H cleavage at the N3 position may also occur following electron transfer from the π^* orbital of the

^aDepartment of Chemistry, University of California, Berkeley, CA 94720, USA. E-mail: dneumark@berkeley.edu

^bChemical Sciences Division, Lawrence Berkeley National Laboratory, Berkeley, CA 94702, USA

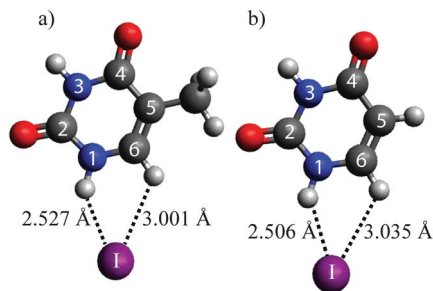


Fig. 1 Structures of a) iodide–thymine and b) iodide–uracil clusters with calculated bond distances indicated.

nucleobase. Understanding the mechanisms driving relaxation and fragmentation of nucleobases subsequent to charge transfer will provide insight into how low energy electrons cause DNA damage. In this article, we explore time-resolved radiation chemistry by performing one-photon photoelectron (PE) spectroscopy and two-color time-resolved PE spectroscopy of iodide–thymine ($I^- \cdot T$) and iodide–uracil ($I^- \cdot U$) complexes, expanding on our previous report of $I^- \cdot U$.¹¹

Extensive experimental and theoretical work has been carried out on the nucleobases of DNA and RNA to gain insight into the mechanisms of DNA damage. Dissociative electron attachment (DEA) experiments examining dissociation pathways of isolated nucleobases as a function of incident electron collision energy^{12–16} find that the dominant channel at low collision energy is production of the deprotonated DNA base ($B-H$)⁻ *via* hydrogen loss from the N1 position. Sharp resonances in the DEA spectra at and just below 1 eV have been attributed to vibrational Feshbach resonances resulting from the coupling of dipole-bound states of the isolated nucleobase to the σ^* orbital of the N1–H bond, leading to fragmentation and hydrogen loss.^{17,18}

PE spectroscopy and Rydberg electron transfer (RET) experiments demonstrate that the anions of the isolated nucleobases are preferentially formed in dipole-bound states rather than conventional valence-bound states.^{19–22} Dipole-bound anions readily form for molecules with dipole moments greater than 2.5 Debye,²³ and isolated nucleobases have dipole moments on the order of 4 D.^{24,25} Bowen and co-workers²⁰ recorded PE spectra characteristic of dipole-bound states for thymine and uracil anions, yielding adiabatic electron affinities (AEAs) for uracil and thymine of 93 ± 7 meV and 69 ± 7 meV, respectively. These spectra are dominated by a single narrow peak representing the transition between the anion and neutral ground vibrational states due to very similar anion and neutral geometries. There is, however, experimental and theoretical evidence of low-lying valence states of nucleobase anions. These species are expected to have relatively broad PE spectra and higher vertical detachment energies (VDEs, defined as the difference in energy between the anion and neutral at the geometry of the anion) than dipole-bound states.²⁶ RET experiments on nucleobases by Schermann and co-workers^{21,22} suggested that valence-bound states of uracil could be formed by electron attachment to $U(Ar)_n$ clusters, followed by Ar evaporation.

Experiments by Bowen¹⁹ on uracil–rare gas binary cluster anions found that the uracil anion remains a dipole-bound state upon complexation with Ar or Kr. However, the PE spectrum of the uracil–Xe anion complex showed evidence of both

a dipole-bound and valence-bound uracil anion, with the latter having a VDE of ~ 0.6 eV. Only the valence-bound state was seen in the binary complex with water. Schiedt *et al.*²⁷ reported PE spectra of anionic DNA bases solvated by one or more water molecules. By extrapolating to zero water molecules, the electron affinities of uracil and thymine to form valence-bound states were estimated to be 150 ± 120 meV and 120 ± 120 meV respectively, within the range of the electron affinity to form dipole-bound states. Calculations report VDEs of the valence-bound anions of 0.5 eV for thymine²⁸ and 0.6 eV for uracil^{29,30} and suggest that a stable valence-bound anion should exist in a puckered ring geometry.²⁶

Here we apply conventional PE spectroscopy and femtosecond time-resolved PE spectroscopy^{31,32} to iodide–thymine ($I^- \cdot T$) and iodide–uracil ($I^- \cdot U$) anion complexes in order to study the energetics and dynamics of nucleobase transient negative ions. Calculated structures, see section 3.3, for both complexes are shown in Fig. 1. Using an ultraviolet pump pulse, the excess electron photo-detached from the iodide can interact with the nucleobase, forming a transient negative ion $I \cdots B^{*-}$ in analogy to electron scattering studies. In the time-resolved experiments, a probe pulse detaches the electron from the transient negative ion of thymine or uracil, yielding the decay times of these species and providing insight into their dynamics. Through these experiments we hope to understand the energetics and dynamics of the thymine and uracil transient negative ions.

2 Experimental details

The experimental apparatus has been described in detail elsewhere.^{33,34} Clusters of $I^- \cdot T$ and $I^- \cdot U$ are produced by passing argon gas at 50 psig over a reservoir containing methyl iodide. This gas mixture is expanded through an Even-Lavie pulsed solenoid valve operating at 500 Hz with a cartridge containing the sample heated to 205 °C. The pulsed beam passes through a ring filament ionizer creating iodide–nucleobase anionic clusters. The anionic clusters are accelerated perpendicularly and separated in time using a Wiley–McLaren time-of-flight (TOF) mass spectrometer.³⁵ The mass spectrum is calibrated using the characteristic peak progression of $I^-(Ar)_n$ clusters. The cluster size of interest is mass-selected and crossed with one or two laser beams perpendicular to the TOF axis. The resulting photoelectrons are accelerated collinearly by a set of velocity map imaging plates³⁶ onto a position sensitive detector consisting of two chevron stacked microchannel plates, a phosphor screen, and a charge-coupled device camera.

The femtosecond laser pulses used in our experiment are generated from a Ti:Sapphire oscillator and multipass amplifier (KM Labs Griffin Oscillator and Dragon Amplifier). The laser operates at a 1 kHz repetition rate and produces 1.8 mJ per pulse centered at 790 nm. An optical chopper reduces the repetition rate of the laser to 500 Hz to match the repetition rate of the pulsed solenoid valve. In order to generate the UV pump wavelengths used in the experiment, a portion of the 790 nm pulse is either frequency-tripled to generate 265 nm or sent into an optical parametric amplifier (Light Conversion TOPAS-C). The output of the TOPAS can be frequency-doubled to produce nearly continuous wavelengths from 235 nm to 330 nm (5.27–3.75 eV), with energies of approximately 10 μ J/pulse. Part of the remaining fundamental at 790 nm (1.57 eV) serves as the probe pulse. Measurements of the cross correlation between the pump and the probe directly before the laser pulses enter the experimental apparatus yield a cross correlation of approximately 150 fs.

The photoelectron images obtained on our detector are reconstructed following four-way symmetrization using the basis-set expansion method (BASEX).³⁷ Both electron kinetic energy (eKE) distributions as well as photoelectron angular distributions (PADs), which will not be considered in this paper, can be obtained from the reconstructed images. The electron kinetic energy distributions were calibrated using the well-known spectrum of iodide.

3 Results

3.1 One-photon photoelectron spectra

Fig. 2a and 2b show one-photon photoelectron spectra for $\text{I}^- \cdot \text{T}$ and $\text{I}^- \cdot \text{U}$ measured at excitation energies ranging from 4.10–5.30 eV. For ease of comparison at different photon energies, the spectra are plotted as a function of electron binding energy, eBE , where $eBE = hv - eKE$. Both the iodide–thymine and iodide–uracil spectra show electron signal due to direct detachment from the anion to the neutral iodine–nucleobase complex (feature A) as well as photoelectrons with nearly zero kinetic energy (feature C), found where $eBE \approx hv$. At 5.30 eV, an additional signal (feature B) is seen. This feature represents detachment to the $^2P_{1/2}$ state of iodine complexed to the nucleobase. Vertical detachment energies of both anions can be derived by fitting feature A with a Gaussian function to find the peak center, yielding values of 4.05 ± 0.05 eV and 4.11 ± 0.05 eV for $\text{I}^- \cdot \text{T}$ and $\text{I}^- \cdot \text{U}$, respectively.

For both anion complexes, feature C is observed as a distinct feature from 5.30 eV to 4.20 eV, a range of 0.90 eV. Near-zero kinetic energy photoelectron signal is observed for excitation energies as low as 3.76 eV for both complexes, but below 4.20 eV only a single peak or rising edge is seen that cannot definitively be assigned as feature A or feature C. Table 1 gives the ratio of intensities of features C and A for both species at excitation energies where both features are seen and clearly defined. This ratio is highest at 4.77 eV for both complexes, although $\text{I}^- \cdot \text{T}$ complexes have consistently higher C/A ratios than $\text{I}^- \cdot \text{U}$ complexes at all photon energies.

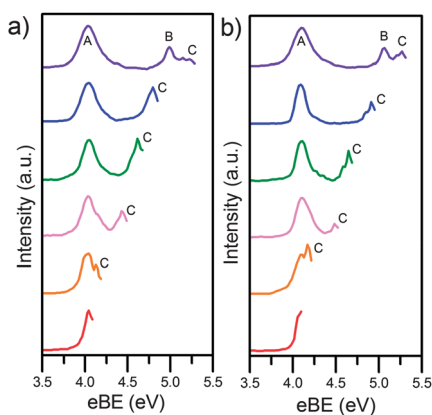


Fig. 2 One-photon photoelectron spectra at different photon energies of iodide–thymine a), and iodide–uracil b), where A indicates photoelectrons from direct detachment to the $^2P_{3/2}$ neutral state and, and B to the $^2P_{1/2}$ neutral state, and C zero kinetic energy electrons. From top to bottom photon energies are as follows in a) 5.30 eV, 4.87 eV, 4.70 eV, 4.51 eV, 4.20 eV, and 4.10 eV and in b) 5.30 eV, 4.92 eV, 4.68 eV, 4.51 eV, 4.20 eV, and 4.10 eV.

Table 1 Ratios of feature C to feature A

Pump energy (eV)	Thymine	Uracil
4.92	—	0.36
4.87	0.56	—
4.77	0.62	0.42
4.70	0.57	—
4.68	—	0.36
4.51	0.33	0.13

3.2 Two-photon time-resolved photoelectron spectra of $I^- \cdot T$ and $I^- \cdot U$

Fig. 3 shows a representative time-resolved photoelectron spectrum of $I^- \cdot T$ excited at 4.79 eV and probed at 1.57 eV, plotting photoelectron signal vs. eKE at a series of pump-probe delays. Three features are apparent in the spectra: the direct detachment feature A, near-zero kinetic energy electrons (feature C), and a broad, low intensity signal (feature D) with eKE ranging between 1.0–1.6 eV. Features A and C appear at all pump-probe delays, while the transient feature D appears at zero pump-probe delay, t_0 , and persists for tens of picoseconds. The rise and decline of the transient feature is mirrored by depletion and subsequent recovery in the intensity of feature C.

Fig. 4 displays the time-dependent integrated intensities of features C and D for $I^- \cdot T$ measured with an excitation energy of 4.69 eV at short and long time delays. The open circles and squares represent measured intensities for features C and D, respectively, while the curves are obtained from the fitting procedure described in the next section. At all pump energies, feature D rises abruptly at t_0 , then decays monotonically over a time scale of 100–300 fs. A more detailed analysis in the next section shows that feature D decays biexponentially at all excitation energies studied. Features C and D show complementary dynamics: feature C has non-zero intensity at negative time delays, is abruptly depleted at t_0 , then recovers on time scales similar to the decay of D. Both signals reach their asymptotic values by 5 ps.

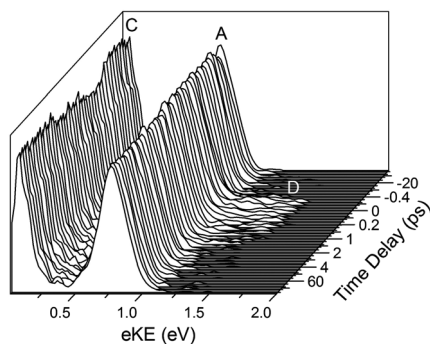


Fig. 3 Time-resolved photoelectron spectrum of the iodide–thymine cluster excited at 4.79 eV and probed at 1.57 eV. Features A, C, and D represent direct detachment of the anion to form the corresponding neutral species, vibrational autodetachment, and photodetachment of the transient negative ion, respectively.

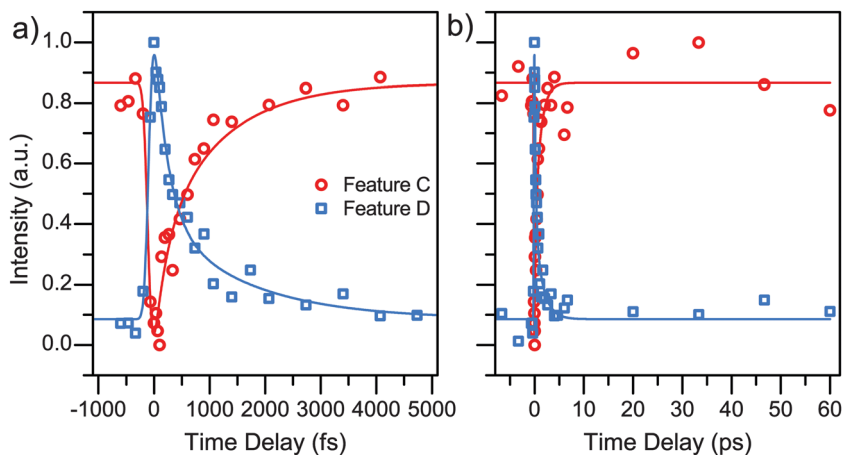


Fig. 4 Normalized integrated intensities for features C and D in $I^- \cdot T$ clusters excited at 4.69 eV and probed at 1.57 eV, where a) shows short time dynamics and b) shows long time dynamics.

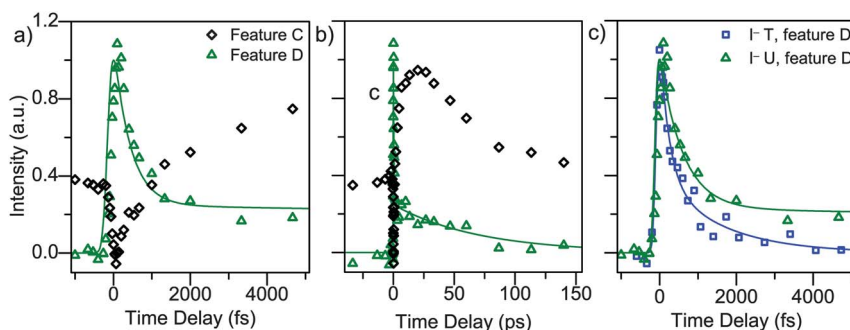


Fig. 5 Normalized integrated intensities for $I^- \cdot U$ clusters excited at 4.69 eV and probed at 1.57 eV where a) shows the short time dynamics of features C and D, b) the long time dynamics and c) a comparison between the short time dynamics of feature D in $I^- \cdot U$ with that of $I^- \cdot T$ excited at 4.69 eV.

Analogous plots for iodide–uracil clusters based on our earlier work¹¹ are presented in Fig. 5a and 5b. As in $I^- \cdot T$, the intensity of feature D sharply increases at t_0 and then undergoes biexponential decay. Fig. 5c compares the short-time dynamics of feature D for $I^- \cdot T$ and $I^- \cdot U$ at the same pump energy, showing slower decay at short times and more persistent signal at longer times for $I^- \cdot U$. Feature C is also quite different in $I^- \cdot U$. While this feature shows similar depletion and recovery for both complexes at early times, it subsequently recovers past its initial intensity in $I^- \cdot U$. Maximum intensity is achieved after about 25 ps, followed by decay to its initial value over tens of picoseconds.

3.3 Electronic structure calculations

The structures of the iodide–nucleobase complexes were optimized using second order perturbation theory in the Gaussian 09 software package³⁸ with an augmented double zeta Dunning-type basis and an aug-cc-pVDZ-pp pseudopotential³⁹ for iodide. Calculated structures of the $I^- \cdot T$ and $I^- \cdot U$ complexes are shown in Fig. 1, with calculated bond distances indicated between iodide and the

N1 and C6 protons. The excess charge is localized on the iodine atom. The iodide resides between the hydrogen bound to N1 and the neighboring vinyl hydrogen in both clusters and appears to interact somewhat more with the hydrogen bound to C6 in the thymine complex than in the uracil complex. The presence of iodide leads to slight elongation of the N1–H and C5–C6 bonds relative to un-complexed species,^{26,40} as well as bowing of both the N1 and C6 hydrogen atoms toward the halide. Single point energy calculations carried out using CCSD with the same basis sets estimate VDEs as 4.09 and 4.13 eV for thymine- and uracil-containing complexes, respectively. The calculated geometry and VDE for $I^- \cdot U$ agree well with a recent calculation by Ortiz⁴¹ using density functional theory.

4 Analysis

The integrated intensity of feature D and, for $I^- \cdot T$, feature C, can be fit to eqn (1), representing a convolution of a Gaussian instrumental response function, with a FWHM of the measured cross correlation of 150 fs, and a step function at $t = t_0$ that then evolves bi-exponentially:

$$I(t) = e^{-t^2/\sigma^2} * \begin{cases} I_0 & t < t_0, \\ I_0 + A_0\delta(t - t_0) + A_1e^{-(t-t_0)/\tau_1} + A_2e^{-(t-t_0)/\tau_2} & t \geq t_0 \end{cases} \quad (1)$$

Table 2 Time constants of feature D in iodide–thymine and iodide–uracil clusters

Nucleobase	Pump energy (eV)	A_1/A_2	τ_1 (fs)	τ_2 (ps)
Thymine	4.60	3.8	300 ± 50	1.9 ± 1.0
	4.69	2.4	200 ± 40	1.5 ± 0.4
	4.79	1.5	160 ± 60	0.9 ± 0.2
Uracil ¹¹	4.69	7.0	620 ± 50	52 ± 20
	4.79	5.6	390 ± 80	37 ± 20
	4.90	5.6	300 ± 50	12 ± 6

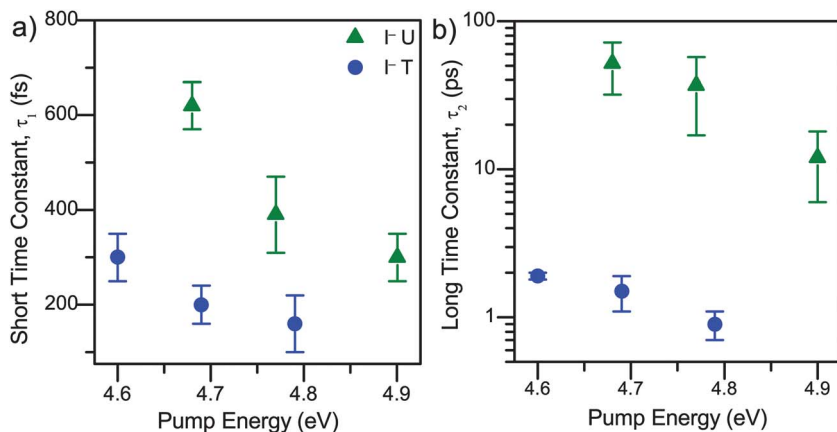


Fig. 6 a) Short and b) long time constants b) in Table 2 versus excitation energy for $I^- \cdot T$ and $I^- \cdot U$ clusters.

Table 2 lists the time constants τ_1 and τ_2 and the amplitude ratio A_1/A_2 for $I^- \cdot T$ and $I^- \cdot U$ at the various excitation energies used in our experiment, while Fig. 6a and 6b plot the two time constants against excitation energy. For both systems, τ_1 and τ_2 decrease with increasing excitation energy. The time constants τ_1 and τ_2 are systematically shorter for $I^- \cdot T$. This trend is particularly striking for τ_2 values, which are over an order of magnitude shorter for $I^- \cdot T$ than for $I^- \cdot U$. Moreover, while the time-dependence of feature C for $I^- \cdot T$ can be completely described by eqn (1) with the same constants that fit feature D (except that A_1 and A_2 are negative), this functional form cannot capture the long-time dynamics of feature C in $I^- \cdot U$.

5 Discussion

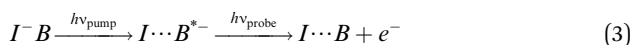
5.1 Nature of iodide–nucleobase clusters

In one-photon PE spectra of both $I^- \cdot T$ and $I^- \cdot U$ at 5.30 eV, the two direct detachment features A and B are split by the spin orbit splitting of iodine, indicating the anion has the electronic character of iodide, and the excess electron in the ground state of these complexes is localized on the iodine atom. This interpretation is fully supported by the electronic structure calculations reported here and elsewhere.⁴¹

The one-photon photoelectron spectra in Fig. 2 show clear evidence of very slow electrons, feature C, over a wide range of excitation energies. This feature is assigned to vibrational autodetachment from the transient negative ion (TNI), $I \cdots B^{*-}$, formed after charge transfer from iodide to the nucleobase, as follows:



The resulting photoelectrons have nearly zero kinetic energy. A similar slow electron signal, seen in our previous work on iodide–solvent clusters, was also ascribed to autodetachment.^{42–45} The TNI is also the source of pump–probe signal observed as feature D in the time-resolved experiments according to:



The resulting photoelectrons are ejected with a kinetic energy given by $eKE = h\nu_{\text{probe}} - VDE(I \cdots B^{*-})$ where the last term is the VDE of the TNI in eqn (3). The eKE of feature D ranges from 1.0–1.6 eV. Owing to the diffuse nature of this transient signal, we cannot definitively assign the VDE of the TNI but can place it in the range of 0–0.6 eV, which includes the calculated VDEs of 0.5 and 0.6 eV for the valence bound anions of thymine and uracil.^{28,26} Notably, we can see no spectroscopic evidence of the sharp peak characteristic of dipole-bound nucleobases at any pump–probe delay. We therefore conclude that the TNI formed in our experiment upon UV initiated charge transfer is the valence-bound state of the nucleobase. Anion photoelectron spectroscopy¹⁹ and Rydberg electron transfer²² experiments show that complexation to a polarizable species stabilizes valence-bound anions relative to dipole-bound states, and we may be seeing a manifestation of that effect here owing to the nearby iodine atom.

Our experiment can be considered in terms of intracluster electron scattering, where the electron produced by photodetachment from the iodide moiety is either ejected into free space, resulting in the direct detachment features A and B,

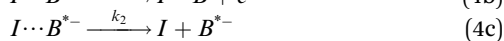
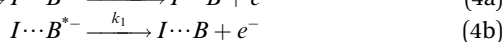
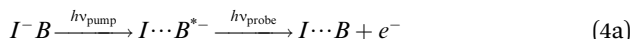
or is indirectly scattered from the nucleobase forming the TNI leading to the time-dependent features C and D. A similar mechanism was also proposed by Continetti and co-workers⁴⁶ in their dissociative photodetachment experiments on the iodide–aniline complex.

Since thymine and uracil absorb at the excitation energies used in our experiment,^{47,48} we must also consider the possibility that UV absorption by the nucleobase could excite the nucleobase to a $\pi \rightarrow \pi^*$ state, followed by transfer of an electron from iodide into the π hole of the nucleobase and forming the same $I \cdots B^{*-}$ state as in in eqn (2) and (3). There are several arguments against this mechanism, however. First, Fig. 4 and 5 show formation of the TNI immediately at t_0 , with an appearance rate limited by the Gaussian shape of our laser pulses, whereas electron transfer from iodide to an electronically excited nucleobase would likely result in delayed formation of the TNI. Secondly, the gas phase absorption cross section for uracil increases by more than a factor of ten from 4.2 to 5.0 eV,⁴⁸ and the gas phase spectrum of thymine also rises steeply above its onset around 4.4 eV.⁴⁹ The autodetachment signal in Fig. 2 does not show a corresponding increase with energy, however, indicating that it is not correlated with UV absorption by the nucleobase.

5.2 Time-resolved dynamics

The transient feature D in the time-resolved photoelectron spectra decays bi-exponentially for both $I^- \cdot T$ and $I^- \cdot U$ clusters. Key trends are shown in Table 2 and Fig. 6a and 6b. For both complexes, the two time constants τ_1 and τ_2 decrease with increasing excitation energy. This result is consistent with a statistical decay process such as vibrational autodetachment in eqn (2), as shown in our recent work on other iodide–solvent clusters.⁵⁰ The fast time constant τ_1 ranges from 150–600 fs. Fig. 6a shows that at comparable excitation energies, τ_1 is more than a factor of two smaller for thymine than uracil complexes. For example, at 4.69 eV, $\tau_1 = 200$ fs for $I^- \cdot T$ but is 620 fs for $I^- \cdot U$. The slow time constant τ_2 varies from 1–2 ps for $I^- \cdot T$ and is considerably longer (12–52 ps) for $I^- \cdot U$.

The bi-exponential decay of feature D indicates that the $I \cdots B^{*-}$ state created by the pump pulse does not decay solely by autodetachment. Instead it must also decay to a longer-lived anion state that can be detached with a 1.57 eV probe photon. In $I^- \cdot T$, recovery of the autodetachment signal C is bi-exponential and it fit well with the same time constants as those used to fit feature D. This correspondence indicates that in $I^- \cdot T$, both the initial $I \cdots B^{*-}$ state and its anionic decay product undergo autodetachment. The situation for autodetachment from the uracil complex is more complicated and is considered in more detail below. An overall mechanism consistent with our results is as follows:



Here, the initially formed $I \cdots B^{*-}$ species can be detached by a probe photon (4a), autodetach (4b), or lose an iodine atom (4c). The B^{*-} fragment from (4c) can also be photodetached by a probe photon (4d) or autodetach (4e). The iodine atom

should be bound to the nucleobase by ~ 50 meV,⁴² so the B^{*-} fragment should have less vibrational energy than the initially formed $I\cdots B^{*-}$ resulting in an autodetachment rate k_3 slower than k_1 . According to this scheme, the two time constants τ_1 and τ_2 are related to the three rate constants in (4) by:

$$\tau_1 = 1/(k_1 + k_2), \tau_2 = 1/k_3 \quad (5)$$

The overall mechanism in eqn (4) explains the decay of feature D in both uracil and thymine and the dynamics of feature C in thymine. However, it does not explain the overshoot in feature C observed in uracil. As has been argued previously,^{11,51} this overshoot indicates enhancement of the autodetachment signal by the probe pulse. Fig. 5b shows that the time interval during which feature C exceeds its initial level roughly coincides with the long-time decay of feature D. Hence, the overshoot may occur through probe absorption by the U^{*-} fragment, produced in step (4c), to an autodetaching state. In other words, the probe pulse may not only induce direct detachment (4d) but may also enhance autodetachment. Once the U^{*-} fragment has decayed by (4e) the probe pulse can no longer be absorbed and the overshoot disappears. Note that because τ_2 is considerably shorter in $I^- \cdot T$, the lifetime of the fragment that absorbs the probe pulse may be too short to see significant probe-enhanced autodetachment, which might explain the absence of this effect in $I^- \cdot T$ complexes.

We should also consider other possible contributions to the time-resolved dynamics seen in our experiments, summarized in Fig. 7 along with previously discussed iodine loss. DEA experiments show that low-energy electron collisions with uracil^{12,52} and thymine⁴⁵ lead to formation of the deprotonated $(U-H)^-$ and $(T-H)^-$ anions *via* hydrogen atom loss from the N1 position. In the low energy regime, the yield for this channel shows an onset of 0.6 eV, a small peak at 0.7 eV

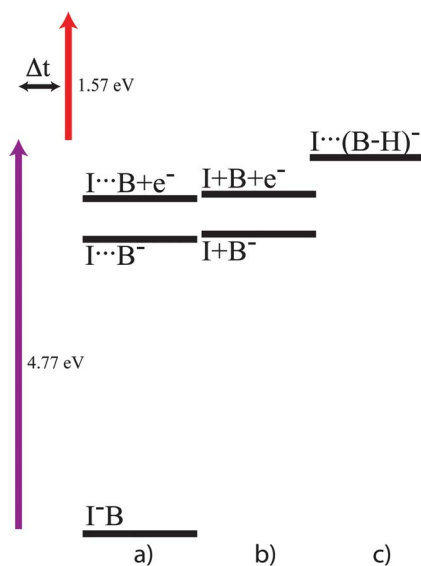


Fig. 7 Energy diagram showing approximate relative energies of possible fragmentation pathways of thymine and uracil subsequent to UV initiated charge transfer from iodide where a) shows UV initiated charge transfer, b) iodine loss, and c) hydrogen loss.

and a much larger resonance at 1 eV.¹⁷ These results raise the question of whether the analogous channel is energetically accessible in our experiments, whereby electron transfer to the nucleobase from the iodide leads to H-atom loss. Calculations by Martínez *et al.*⁴¹ find that removal of a hydrogen atom from the N1 position in $I^- \cdot U$ requires 4.6 eV, which falls in the range of excitation energies used in our experiments. Alternatively, from the intracuster electron scattering perspective, the electron produced by photodetachment of the iodide moiety collides with the nucleobase at an effective collision energy $E_c = h\nu - VDE(I^- \cdot B)$. The VDEs, as discussed above, are 4.05 eV for $I^- \cdot T$ and 4.11 eV for $I^- \cdot U$. Based on the pump energies in Table 2, the range of E_c is 0.55–0.74 eV and 0.57–0.79 eV for $I^- \cdot T$ and $I^- \cdot U$, respectively, overlapping the threshold for H atom loss in both cases.

It thus appears that H-atom loss is a viable decay channel that can occur in parallel with autodetachment, affecting the decay constants τ_1 and τ_2 . Unfortunately, we are unable to observe this channel directly in our current experimental configuration. Photoelectron spectroscopy experiments on deprotonated thymine find that the electron affinity of the T-H radical is 3.25 eV,⁵³ and one can reasonably assume a similar value for U-H. Therefore the probe energy in our experiment, 1.57 eV, is not sufficient to detach these species and the excess electron is too tightly bound to autodetach. Experiments at higher probe energies will need to be performed in order to assess the importance of this channel. A more indirect approach would be to perform the same experiments reported here on deuterated thymine and uracil. DEA experiments on deuterated thymine show a 40-fold drop in deuterium loss at low energies, compared to hydrogen loss in native thymine.¹⁶ A similar effect is predicted in calculations on uracil.¹⁸ This dramatic isotope effect is attributed to a lower tunneling probability for D-atom loss, whereas autodetachment is unaffected. Hence, if H-atom loss is significant in our experiments, we should see considerably slower decay of the transient feature D upon deuteration as the hydrogen loss channel would be largely turned off.

The possible role of anion tautomerization should also be considered. PES experiments by Bowen and co-workers²⁹ using a laser ablation ionization source found a uracil anion with a VDE of 2.5 eV. Comparison to electronic structure calculations suggests this species is a tautomer of the uracil anion in which a hydrogen atom has migrated from N3 to C5. Several other tautomers have been identified in calculations on uracil and thymine anions.^{54,55} All hydrogen migration tautomers have higher VDEs than the canonical tautomer, and one (the N1-C5 tautomer) is predicted to be more stable than the canonical tautomer by 1.4 kcal mol⁻¹ for thymine and 2.6 kcal mol⁻¹ for uracil. One can envision a scenario in our experiment in which electron transfer from the iodide to the nucleobase is followed by tautomerization to a species with a higher VDE than the initially formed TNI. Such a process would contribute to the decay of the transient feature D. However, the barriers to tautomerization are calculated to be 40 kcal mol⁻¹,^{54,55} and are not accessible in our experiment. Therefore, absent a lower energy path, it is unlikely that tautomerization can occur under the conditions of our experiment. As with H-atom loss, further experiments with higher photon energies should be able to verify the absence of tautomerization.

Given the similarities between uracil and thymine, the observation of considerably faster decay dynamics in $I^- \cdot T$ complexes compared to $I^- \cdot U$ is

striking. The electronic structure of the two nucleobases is similar, as are the DEA cross sections for H atom loss. The additional methyl group in thymine might be expected to slow, rather than accelerate, the autodetachment rate owing to a larger density of reactant states in the TNI. However, our previous work on iodide–solvent clusters showed that relatively small increases in the energy available for autodetachment can significantly raise the autodetachment rate.⁵⁰ Such an effect may be operative here as well. The VDEs of the valence-bound states of thymine and uracil are calculated to be 0.5 and 0.6 eV, respectively,^{26,28,30} while the VDE of $I^- \cdot T$ is 0.06 eV lower than that of $I^- \cdot U$. Therefore at the same excitation energy, there is 0.16 eV more energy available for autodetachment in $I^- \cdot T$ than in $I^- \cdot U$, possibly leading to more rapid autodetachment and faster decay in $I^- \cdot T$.

6 Conclusion

We have investigated the energetics and dynamics of the $I^- \cdot T$ and $I^- \cdot U$ binary clusters using one-photon and two-photon time-resolved photoelectron spectroscopy. The one-photon experiments show a stabilization of iodide by the nucleobase, increasing the VDE from 3.05 eV for bare iodide to 4.11 eV for $I^- \cdot U$ clusters and 4.05 eV for $I^- \cdot T$ clusters. In addition to direct detachment from the anionic cluster to the neutral manifold, we observe a wavelength-independent zero electron kinetic energy feature that we attribute to charge transfer from iodide to the nucleobase, forming a transient negative ion that decays by vibrational autodetachment.

Two-photon time resolved experiments on the $I^- \cdot U$ and $I^- \cdot T$ clusters show that the TNI formed by charge transfer has a VDE between 0–0.6 eV. In both thymine and uracil clusters, this transient feature decays bi-exponentially at all pump energies studied, 4.60–4.90 eV. The short time constants range between 160–300 fs in thymine and 300–600 fs in uracil, while the long time constants range between 1–2 ps in thymine and 12–52 ps in uracil. The bi-exponential decay is attributed to changing rates of autodetachment upon iodine loss from the TNI. The shorter time constants in $I^- \cdot T$ clusters may reflect small differences in the iodide–nucleobase binding energy and the VDE of the nucleobase valence anion. The role of hydrogen atom loss and tautomerization merit further exploration. In addition, more detailed theoretical work into the nature of the iodide–nucleobase interaction both in the ground and charge transfer state would be of considerable interest both for understanding the dynamics observed in this experiment as well as how these experiments can be used to provide insight into the interactions of excess electrons with DNA.

Acknowledgements

This research is supported by the National Science Foundation (NSF) under grant CHE-1011819. S.B.K. and M.A.Y. are grateful for funding through NSF Graduate Research Fellowships.

References

- 1 C. von Sonntag, *Chemical Basis of Radiation Biology*, Taylor and Francis, London, 1987.
- 2 H. Schussler, S. Navaratnam and L. Distel, *Radiat. Phys. Chem.*, 2005, **73**, 163–168.
- 3 N. S. Hush and A. S. Cheung, *Chem. Phys. Lett.*, 1975, **34**, 11–13.

- 4 A. O. Colson, B. Besler and M. D. Sevilla, *J. Phys. Chem.*, 1993, **97**, 8092–8097.
- 5 K.-W. Choi, J.-H. Lee and S. K. Kim, *J. Am. Chem. Soc.*, 2005, **127**, 15674–15675.
- 6 K. B. Bravaya, O. Kostko, S. Dolgikh, A. Landau, M. Ahmed and A. I. Krylov, *J. Phys. Chem. A*, 2010, **114**, 12305–12317.
- 7 D. Ghosh, A. Golan, L. K. Takahashi, A. I. Krylov and M. Ahmed, *J. Phys. Chem. Lett.*, 2011, **3**, 97–101.
- 8 B. Boudaiffa, P. Cloutier, D. Hunting, M. A. Huels and L. Sanche, *Science*, 2000, **287**, 1658–1660.
- 9 J. Simons, *Acc. Chem. Res.*, 2006, **39**, 772–779.
- 10 J. Gu, Y. Xie and H. F. Schaefer, *J. Am. Chem. Soc.*, 2006, **128**, 1250–1252.
- 11 M. A. Yandell, S. B. King and D. M. Neumark, *J. Am. Chem. Soc.*, 2013, **135**, 2128–2131.
- 12 G. Hanel, B. Gstir, S. Denifl, P. Scheier, M. Probst, B. Farizon, M. Farizon, E. Illenberger and T. D. Märk, *Phys. Rev. Lett.*, 2003, **90**, 188104.
- 13 A. M. Scheer, C. Silvernail, J. A. Belot, K. Aflatooni, G. A. Gallup and P. D. Burrow, *Chem. Phys. Lett.*, 2005, **411**, 46–50.
- 14 S. Ptasíńska, S. Denifl, V. Grill, T. D. Märk, E. Illenberger and P. Scheier, *Phys. Rev. Lett.*, 2005, **95**, 093201.
- 15 S. Ptasíńska, S. Denifl, B. Mróz, M. Probst, V. Grill, E. Illenberger, P. Scheier and T. D. Märk, *J. Chem. Phys.*, 2005, **123**, 124302.
- 16 S. Denifl, P. Sulzer, F. Zappa, S. Moser, B. Kräutler, O. Echt, D. K. Bohme, T. D. Märk and P. Scheier, *Int. J. Mass Spectrom.*, 2008, **277**, 296–299.
- 17 P. D. Burrow, G. A. Gallup, A. M. Scheer, S. Denifl, S. Ptasíńska, T. Märk and P. Scheier, *J. Chem. Phys.*, 2006, **124**, 124310.
- 18 G. A. Gallup and I. I. Fabrikant, *Phys. Rev. A: At., Mol., Opt. Phys.*, 2011, **83**, 012706.
- 19 J. H. Hendricks, S. A. Lyapustina, H. L. de Clercq and K. H. Bowen, *J. Chem. Phys.*, 1998, **108**, 8–11.
- 20 J. H. Hendricks, S. A. Lyapustina, H. L. de Clercq, J. T. Snodgrass and K. H. Bowen, *J. Chem. Phys.*, 1996, **104**, 7788–7791.
- 21 C. Desfrancois, H. Abdoul-Carime and J. P. Schermann, *J. Chem. Phys.*, 1996, **104**, 7792–7794.
- 22 C. Desfrancois, V. Periquet, Y. Bouteiller and J. Schermann, *J. Phys. Chem. A*, 1998, **102**, 1274–1278.
- 23 O. H. Crawford, *Mol. Phys.*, 1971, **20**, 585–591.
- 24 R. D. Brown, P. D. Godfrey, D. McNaughton and A. P. Pierlot, *J. Am. Chem. Soc.*, 1988, **110**, 2329–2330.
- 25 N. A. Oylar and L. Adamowicz, *J. Phys. Chem.*, 1993, **97**, 11122–11123.
- 26 R. A. Bachorz, W. Klopper and M. Gutowski, *J. Chem. Phys.*, 2007, **126**, 085101.
- 27 J. Schiedt, R. Weinkauff, D. M. Neumark and E. Schlag, *Chem. Phys.*, 1998, **239**, 511–524.
- 28 D. Svozil, T. Frigato, Z. k. Havlas and P. Jungwirth, *Phys. Chem. Chem. Phys.*, 2005, **7**, 840–845.
- 29 R. A. Bachorz, W. Klopper, M. Gutowski, X. Li and K. H. Bowen, *J. Chem. Phys.*, 2008, **129**, 054309.
- 30 P. Dedíková, L. Demovič, M. Pitoňák, P. Neogrady and M. Urban, *Chem. Phys. Lett.*, 2009, **481**, 107–111.
- 31 T. Suzuki and B. J. Whitaker, *Int. Rev. Phys. Chem.*, 2001, **20**, 313.
- 32 A. Stolow, A. E. Bragg and D. M. Neumark, *Chem. Rev.*, 2004, **104**, 1719–1757.
- 33 A. V. Davis, R. Wester, A. E. Bragg and D. M. Neumark, *J. Chem. Phys.*, 2003, **118**, 999–1002.
- 34 A. E. Bragg, J. R. R. Verlet, A. Kammrath, O. Cheshnovsky and D. M. Neumark, *J. Am. Chem. Soc.*, 2005, **127**, 15283–15295.
- 35 W. C. Wiley and I. H. McLaren, *Rev. Sci. Instrum.*, 1955, **26**, 1150–1157.
- 36 A. T. J. B. Eppink and D. H. Parker, *Rev. Sci. Instrum.*, 1997, **68**, 3477–3484.
- 37 V. Dribinski, A. Ossadtchi, V. Mandelshtam and H. Reisler, *Rev. Sci. Instrum.*, 2002, **73**, 2634–2642.
- 38 M. J. Frisch, G. W. Trucks, H. B. Schlegel, G. E. Scuseria, M. A. Robb, J. R. Cheeseman, G. Scalmani, V. Barone, B. Mennucci, G. A. Petersson, H. Nakatsuji, M. Caricato, X. Li, H. P. Hratchian, A. F. Izmaylov, J. Bloino, G. Zheng, J. L. Sonnenberg, M. Hada, M. Ehara, K. Toyota, R. Fukuda, J. Hasegawa, M. Ishida, T. Nakajima, Y. Honda, O. Kitao, H. Nakai, T. Vreven, J. A. Montgomery, Jr., J. E. Peralta, F. Ogliaro, M. Bearpark, J. J. Heyd, E. Brothers, K. N. Kudin, V. N. Staroverov, R. Kobayashi, J. Normand, K. Raghavachari, A. Rendell, J. C. Burant, S. S. Iyengar, J. Tomasi, M. Cossi, N. Rega, J. M. Millam, M. Klene, J. E. Knox, J. B. Cross, V. B. Bakken, C. Adamo, J. Jaramillo, R. Gomperts, R. E. Stratmann, O. Yazyev, A. J. Austin, R. Cammi, C. Pomelli, J. W. Ochterski, R. L. Martin, K. Morokuma, V. G. Zakrzewski, G. A. Voth, P. Salvador, J. J. Dannenberg, S. Dapprich, A. D. Daniels, Farkas,

- J. B. Foresman, J. V. Ortiz, J. Cioslowski and D. J. Fox, *Gaussian 09*, Gaussian Inc. Wallingford CT2009.
- 39 K. A. Peterson, B. C. Shepler, D. Figgen and H. Stoll, *J. Phys. Chem. A*, 2006, **110**, 13877–13883.
- 40 L. T. M. Profeta, J. D. Larkin and H. F. Schaefer, *Mol. Phys.*, 2003, **101**, 3277–3284.
- 41 A. Martínez, O. Dolgounitcheva, V. G. Zakrzewski and J. V. Ortiz, *J. Phys. Chem. A*, 2008, **112**, 10399–10404.
- 42 A. Kammrath, J. R. R. Verlet, A. E. Bragg, G. B. Griffin and D. M. Neumark, *J. Phys. Chem. A*, 2005, **109**, 11475–11483.
- 43 O. T. Ehrler, G. B. Griffin, R. M. Young and D. M. Neumark, *J. Phys. Chem. B*, 2009, **113**, 4031–4037.
- 44 R. M. Young, M. A. Yandell and D. M. Neumark, *J. Chem. Phys.*, 2011, **134**, 124311.
- 45 R. M. Young, R. J. Azar, M. A. Yandell, S. B. King, M. Head-Gordon and D. M. Neumark, *Mol. Phys.*, 2012, **110**, 1787–1799.
- 46 M. S. Bowen, M. Becucci and R. E. Continetti, *J. Chem. Phys.*, 2006, **125**, 133309.
- 47 L. B. Clark, G. G. Peschel and I. Tinoco, *J. Phys. Chem.*, 1965, **69**, 3615–3618.
- 48 M. Barbatti, A. J. A. Aquino and H. Lischka, *Phys. Chem. Chem. Phys.*, 2010, **12**, 4959–4967.
- 49 B. B. Brady, L. A. Peteanu and D. H. Levy, *Chem. Phys. Lett.*, 1988, **147**, 538–543.
- 50 M. A. Yandell, R. M. Young, S. B. King and D. M. Neumark, *J. Phys. Chem. A*, 2012, **116**, 2750–2757.
- 51 O. Kornilov, O. Bunermann, D. J. Haxton, S. R. Leone, D. M. Neumark and O. Gessner, *J. Phys. Chem. A*, 2011, **115**, 7891–7900.
- 52 S. Denifl, S. Ptasińska, G. Hanel, B. Gstir, M. Probst, P. Scheier and T. D. Märk, *J. Chem. Phys.*, 2004, **120**, 6557–6565.
- 53 B. F. Parsons, S. M. Sheehan, T. A. Yen, D. M. Neumark, N. Wehres and R. Weinkauff, *Phys. Chem. Chem. Phys.*, 2007, **9**, 3291–3297.
- 54 R. A. Bachorz, J. Rak and M. Gutowski, *Phys. Chem. Chem. Phys.*, 2005, **7**, 2116–2125.
- 55 K. Mazurkiewicz, R. A. Bachorz, M. Gutowski and J. Rak, *J. Phys. Chem. B*, 2006, **110**, 24696–24707.